ACS APPLIED MATERIALS & INTERFACES

Research Article

www.acsami.org

TiO_2–$BiVO_4$ Heterostructure to Enhance Photoelectrochemical Efficiency for Sensitive Aptasensing

Pei Pei Liu,[†] Xiaoqiang Liu,*[,†] Xiao He Huo,[†] Yunfei Tang,[†] Jun Xu,[†] and Huangxian Ju*[,‡]

[†]Institute of Environmental and Analytical Sciences, College of Chemistry and Chemical Engineering, Henan University, Kaifeng, Henan Province 475004, P. R. China

[‡]State Key Laboratory of Analytical Chemistry for Life Science, Department of Chemistry, Nanjing University, Nanjing 210023, P. R. China

ABSTRACT: This work designed a nanocomposite to enhance the photoelectrochemical (PEC) efficiency by depositing $BiVO_4$ nanoparticles on TiO_2 nanospheres with a solvothermal method. The TiO_2–$BiVO_4$ heterostructure was characterized with various spectroscopic and microscopic techniques and was employed as a nanostructured support to cross-link DNA aptamer for constructing a visible-light driven PEC aptasensor. The TiO_2 nanospheres provided a biocompatible microenvironment, and the high surface area of the heterostructure enhanced the loading of aptamer molecules. The small energy gap of $BiVO_4$ improved the PEC property of the nanocomposite compared with the pure TiO_2 under visible-light irradiation. The advantages of the nanocomposite along with the high loading of recognition molecules greatly improved the sensitivity of the aptasensor. Using 17β-estradiol as an analyst model, the proposed PEC biosensor showed excellent analytical performance with high sensitivity, low detection limit of 0.022 pM, and high selectivity in a detectable concentration range of 0.1–250 pM, indicating the promising application of the designed TiO_2–$BiVO_4$ heterostructure in PEC biosensing.

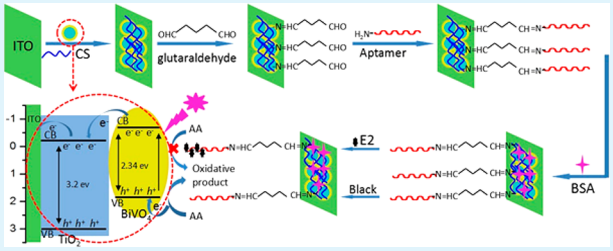

KEYWORDS: *TiO_2–$BiVO_4$ heterostructure, photoelectrochemical aptasensor, sensitization, DNA aptamers, nanobiosensing, 17β-estradiol*

INTRODUCTION

Steroid hormones have attracted great attention in environmental and biomedical fields due to their harmful effects on the endocrine function of human and animals.[1] For example, the presence of a low concentration of estrogens in the environment can cause abnormal sexual development of animals and decrease the average numbers of human spermatozoa.[2,3] Therefore, highly sensitive and selective detection of estrogens in aquatic environments is of great importance to protect the health of humans and animals. The classical method for determination of estrogens is high-performance liquid chromatography,[1] but this technology requires rather complicated instrumentations, intensive labor, and a large amount of time. With the achievements of nanotechnology and nanoscience, nanobiosensing opens up the novel avenue for sensitive biosensing in clinical, environmental, and industrial applications. Some electrochemical biosensors based on nanotechnology have been developed for sensitive detection of estrogen.[1] However, specific biosensors with high sensitivity for estrogen detection are still in urgent demand.

As a fast growing analytical technique, photoelectrochemical (PEC) detection has been paid great attention owing to its desirable signal-to-noise ratio, low cost, and fast detection speed.[4,5] However, the poor sensitivity and selectivity of PEC sensors has restricted their further practical applications. To improve the sensitivity, various semiconductors, especially TiO_2-based composites have been applied in the construction of photocatalysts, photovoltaic devices and biosensors owing to their high photon-to-electron conversion efficiency, excellent biocompatibility, and remarkable chemical stability.[6] However, TiO_2 can only be excited by ultraviolet light (<387 nm), which occupies less than 5% of the solar light spectrum. In addition, photoinduced hole–electron pairs in TiO_2 semiconductors are subjected to fast recombination.[7] The ideal way of minimizing these drawbacks is to combine other visible-light driven semiconductors with TiO_2. For example, Zhang et al.[2,8] synthesized a graphene-TiO_2 nanocomposite as a visible light photocatalyst for selective oxidation of alcohols under mild conditions. The composite exhibited a much more active visible light photocatalytic activity than pure TiO_2. Inspired by this report, this work made use of the small band gap (~2.4 eV) of monoclinic $BiVO_4$ that has shown strong visible light excitation capability[9,10] to design a novel nanocomposite by depositing $BiVO_4$ nanoparticles on TiO_2 nanospheres with a solvothermal method. TiO_2 nanospheres were initially prepared by a sol–gel method. The relatively high conduction band (CB) edge position of $BiVO_4$ nanoparticles can facilitate the charge transfer when they are composited with other photomaterials

Received: May 19, 2017
Accepted: July 31, 2017
Published: July 31, 2017

DOI: 10.1021/acsami.7b07047
ACS Appl. Mater. Interfaces 2017, 9, 27185–27192

Scheme 1. (A) Synthesis of TiO_2−$BiVO_4$ Composite and (B) Fabrication Procedure of Aptasensor and Photoelectrochemical Mechanism in 0.1 M PBS Containing 0.1 M AA

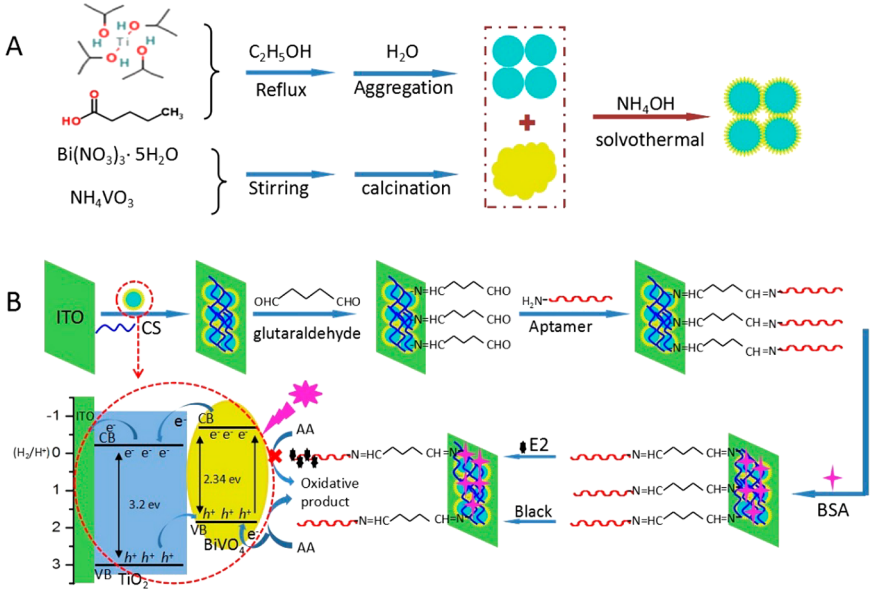

with lower CB position.[11] The nanostructure of $BiVO_4$ avoids rapid recombination of photogenerated charges and poor charge transfer property of bulky $BiVO_4$.[12,13] The advantages of a nanocomposite with strong visible light absorption led to high PEC efficiency for sensitive biosensing.

To obtain a specific response, this work further immobilized DNA aptamer on TiO_2−$BiVO_4$ heterostructure modified indium tin oxide (ITO) to recognize the target. Aptamers are artificial single-stranded DNA or RNA oligonucleotieds, which can selectively recognize various targets including small species, sugars, proteins, and even whole cells,[14,15] and have shown superiority over the traditional recognition elements such as antibodies due to their unique features including simple preparation, easy preservation, good reproducibility, reversible denaturation, stability against high temperature and extreme pH, and particularly target versatility.[7,16] It has been increasingly used as an attractive recognition element for the development of aptasensors.[2] Using 17β-estradiol (E2) as a model analyte, the fabricated PEC aptasensor showed excellent analytical performance over other PEC sensors. The high sensitivity and selectivity for detection of the target indicated the promising application of the designed TiO_2−$BiVO_4$ heterostructure in PEC biosensing.

EXPERIMENTAL SECTION

Material and Reagents. All reagents were commercially available as analytical reagent grade and used as received unless otherwise stated. $Bi(NO_3)_3{\cdot}5H_2O$, NH_4VO_3, and ascorbic acid (AA) were purchased from Sinopharm Chemical Reagent Co., Ltd. (Shanghai, PR China). Titanium isopropoxide (TTIP, 97%+) and valeric acid were purchased from Alfa Aesar (China) Chemicals Co., Ltd. Chitosan (CS, 85% deacetylation) was ordered from Sigma-Aldrich Chemical Co. (St. Louis, MO). Ammonia (28%), glutaraldehyde (50%), 1-amino-anthraquinone, and bisphenol A were obtained from J&K Scientific Ltd. (Beijing, China). 17β-Estradiol (E2), estriol, ethinylestradiol, testosterone, and bovine serum albumin (BSA) were purchased from Shanghai Sangon Biological Engineering Technological Co. Ltd. (Shanghai, China). The amino modified oligonucleotides were purchased from Shanghai Sangon Biotechnology Co. Ltd. (Shanghai, China) with the following sequence: 5′-GCT-TCC-AGC-TTA-TTG-AAT-TAC-ACG-CAG-AGG-GTA-GCG-GCT-CTG-CGC-ATT-CAA-TTG-CTG-CGC-GCT-GAA-GCG-CGG-AAG-C-3′. The aptamer was dissolved in phosphate buffer saline (PBS, pH 7.4) and kept frozen. In this work, 0.1 mol L^{-1} PBS (pH 7.4) was always employed as the supporting electrolyte for PEC determination. Ultrapure water obtained from a Millipore water purification system (≥18 MΩ cm^{-1}, Milli-Q, Millipore) was used throughout the whole experiments.

Apparatus. PEC measurements were performed in a conventional three-electrode system consisting of a modified ITO as the working electrode, a platinum wire as the auxiliary electrode, and a saturated AglAgCl electrode (3.0 M KCl) as the reference electrode. Potential was applied by a CHI630D Electrochemical Workstation (Shanghai CH Instruments, China), and a Xe lamp equipped with a 400 nm cut off filter (CEL-HXUV 300, Beijing AULTT, China) was used as the irradiation source. ITO electrodes were ordered from Wuhan Lattice Solar Energy Technology, Ltd., China. The morphology of the nanomaterials was examined by scanning electron microscopy (SEM, JSM-7500F, JEOL., Japan), transmision electron microscope (TEM, Tecnai G2 20, U.S.A.), and X-ray powder diffraction (XRD, X-PertPro, Netherland) with Cu Kα radiation (λ = 1.5406 nm). UV−vis diffuse reflectance spectra of the samples were measured on an UV−vis spectrophotometer (DRS, UV-2600, Kyoto, Japan). XPS were collected on an X-ray photoelectron spectrometer (ESCALAB 250Xi, U.S.A.) with a monochromated Al Kα source ($h\nu$ = 1486.6 eV), 150 W power, and 500 mm beam spot. The spectra were calibrated on the C 1s peak (284.8 eV) and analyzed with XPSPEAK41 software.

Preparation of TiO_2−$BiVO_4$ Composite. The synthesis of the TiO_2−$BiVO_4$ composite is illustrated in Scheme 1A. In brief, 0.585 g of NH_4VO_3 and 2.425 g of $Bi(NO_3)_3{\cdot}5H_2O$ were added into 100 mL of water under stirring to produce a yellow precipitate, which was then filtered, washed with water, and dried overnight at 60 °C. Subsequently, the resulting product was placed into an alumina crucible and heated to 500 °C for 4 h to obtain the monoclinic $BiVO_4$. The precursor TiO_2 spheres were synthesized using a sol−gel method.[17] First, 0.9 mL of valeric acid was added into 60 mL of ethanol, followed by the addition of 0.9 mL of TTIP to obtain a mixed solution, which was then stirred vigorously and heated at 80 °C for 6 h under reflux in the air. Next, hydrolysis and condensation were initiated by adding 6 mL of water and 30 mL of ethanol into the refluxed solution. After reaction for 4 h, precursor TiO_2 spheres were precipitated, centrifuged, and then washed several times with ethanol

DOI: 10.1021/acsami.7b07047
ACS Appl. Mater. Interfaces 2017, 9, 27185−27192

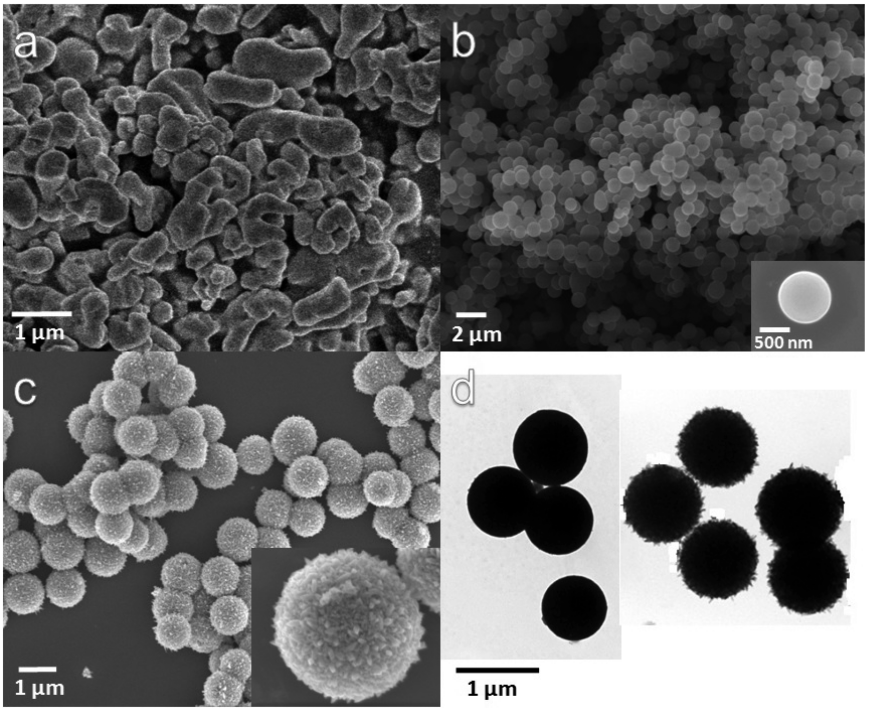

Figure 1. SEM images of (a) $BiVO_4$, (b) precursor TiO_2, and (c) the TiO_2–$BiVO_4$ composite and (d) TEM images of precursor TiO_2 (left) and the TiO_2–$BiVO_4$ composite (right).

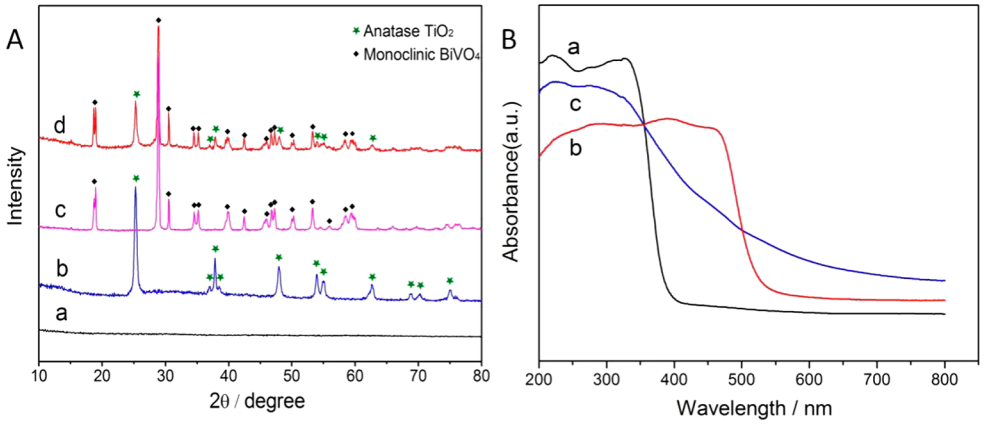

Figure 2. (A) XRD patterns of (a) precursor TiO_2, (b) anatase TiO_2, (c) $BiVO_4$, and (d) the TiO_2–$BiVO_4$ composite and (B) UV–vis diffuse reflectance spectra of (a) anatase TiO_2, (b) $BiVO_4$, and (c) the TiO_2–$BiVO_4$ composite.

and water. Finally, 0.2 g of precursor TiO_2 spheres, 0.04 g of $BiVO_4$, and 1.2 mL of NH_4OH (28% in water) were successively dispersed in a solution of 8 mL of water and 30 mL of ethanol. The dispersion was vigorously stirred for 1 h and then transferred to a 50 mL Teflon-lined stainless steel autoclave kept in an oven at 160 °C for 16 h. The TiO_2–$BiVO_4$ composite was obtained after the dispersion was centrifuged, washed in ethanol, and dried in an oven at 60 °C overnight.

Preparation of PEC Aptasensor. ITO electrode was cleaned with NaOH (1 M) and H_2O_2 (30%) and then washed successively with acetone, alcohol, and water under sonification before use. The TiO_2–$BiVO_4$ composite (2 mg) was dispersed in 1 mL (0.1% w/v) of chitosan aqueous solution containing 1% acetic acid for 1 h to obtain a suspension, 50 μL of which was then applied on ITO. After drying, TiO_2–$BiVO_4$|ITO was immersed into 2.5% (v/v) glutaraldehyde in water for 1 h and thoroughly cleaned to remove the physically absorbed glutaraldehyde. Subsequently, 50 μL of aptamer (2 μM) was covalently immobilized onto the TiO_2–$BiVO_4$|ITO, which was then rinsed with PBS to remove the unbound aptamer and immersed into the BSA solution 3% (w/v) for 1 h to block nonspecific binding sites. The obtained aptasensor was stored at 4 °C overnight until use. The procedure for the biosensor fabrication is illustrated in Scheme 1B.

PEC Measurements. The PEC tests were performed in PBS (0.1 M, pH 7.4) solution containing 0.1 M KCl and 0.1 M AA at a bias voltage of 0.6 V with increasing concentration of E2. The current–time plots were recorded as the visible excitation light was switched on and off. Herein, AA served as an electron donor for capturing photogenerated holes to maintain the photocurrent stability of the PEC aptasensor.

RESULTS AND DISCUSSION

Characterization of Prepared Materials. The SEM and TEM images of $BiVO_4$, precursor TiO_2, and the TiO_2–$BiVO_4$ composite were displayed to characterize their morphologies (Figure 1). The $BiVO_4$ sample was composed of irregular particles with an average diameter of ~1 μm (Figure 1a). The precursor TiO_2 sample consisted of uniform monodisperse beads with very smooth surfaces (Figure 1b). From the

DOI: 10.1021/acsami.7b07047
ACS Appl. Mater. Interfaces 2017, 9, 27185–27192

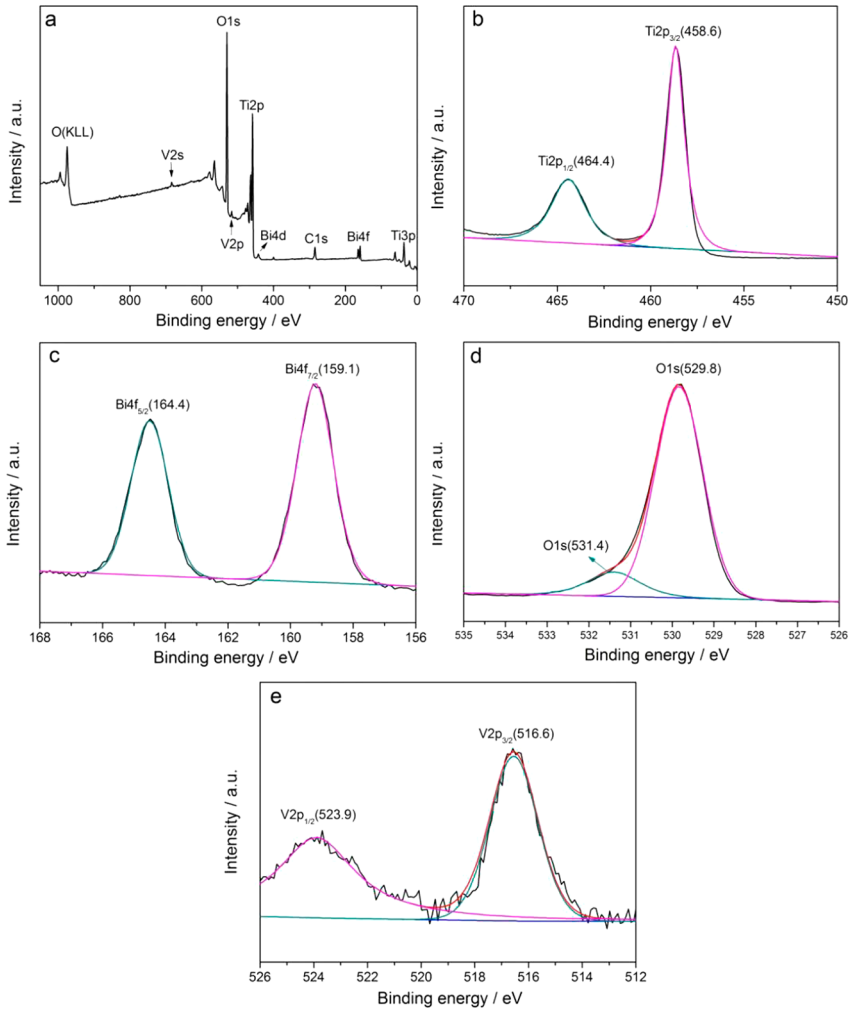

Figure 3. (a) XPS survey scan of the TiO_2−$BiVO_4$ composite and high-resolution XPS spectra of (b) Ti 2p, (c) Bi 4f, (d) O 1s, and (e) V 2p.

magnified image of the precursor TiO_2 beads (inset of Figure 1b), the average diameter of these TiO_2 microspheres was estimated to be 800 ± 50 nm. After the solvothermal treatment, the smooth precursor TiO_2 beads were transformed to the microspheres with rough surface and larger average diameter (1000 ± 50 nm), indicating the deposition of $BiVO_4$ nanoparticles on TiO_2 spheres (Figure 1c). The TEM images (Figure 1d) of precursor TiO_2 (left part) and the TiO_2−$BiVO_4$ composite (right part) provided similar results as the previous SEM images (Figure 1b,c), which also confirmed the formation of the binary heterostructure. In addition, the SEM and TEM photos demonstrated the intimate contact between TiO_2 and $BiVO_4$, which facilitates the electron transfer within the binary composite and improves the separation of photogenerated charges.

The XRD pattern of precursor TiO_2 did not show any obvious diffraction peaks (Figure 2A, curve a), indicating the amorphous structure of these TiO_2 spheres.[9] On the contrary, anatase TiO_2 exhibited several typical peaks at 25.3°, 37.8°, 48.0 °, 53.9 °, 55.1°, and 62.7° (Figure 2A, curve b), corresponding to the (101), (004), (200), (105), (211), and (204) crystal planes (JCPDS card 21-1272).[10] The XRD pattern of $BiVO_4$ showed the peaks at 18.9°, 28.8°, 30.5°, 34.5°, 39.8°, 46.6°, 47.3°, 53.2°, and 55.9° (Figure 2A, curve c), which could be indexed to the characteristic (011), (112), (004), (200), (211), (204), (024), (116), and (215) crystal planes of monoclinic $BiVO_4$ (JCPDS No.14-0688), respectively.[18] Importantly, the XRD pattern of the TiO_2−$BiVO_4$ composite showed almost all of the typical peaks ascribing to both anatase TiO_2 and monoclinic $BiVO_4$ (Figure 2A, curve d), demonstrating the TiO_2 crystal transformation from amorphous to anatase and the successful deposition of monoclinic $BiVO_4$ on TiO_2 nanospheres. However, the peak intensity of $BiVO_4$ in curve d was obviously smaller than that in curve c, most likely due to the low percentage composition of $BiVO_4$ in the composite.

The DRS spectrum of anatase TiO_2 showed the absorption edge at 387 nm (Figure 2B, curve a). According to the Scherer equation, $\lambda = 1240/E_g$ (λ was the absorption edge wavelength),[19] the band gap energy (E_g) was estimated to be 3.2 eV. From the UV−vis absorption edge of the prepared $BiVO_4$ at 530 nm (Figure 2B, curve b), $BiVO_4$ was a visible light absorber with an E_g of 2.34 eV. Compared to the spectrum of anatase TiO_2, the absorption edge of the TiO_2−$BiVO_4$ composite (Figure 2B, curve c) was extended into the visible light region up to ~650 nm, which demonstrated the visible light adsorption capability of the composite.

The XPS measurements were also conducted to investigate the elemental composition of the composite. The XPS survey spectrum of TiO_2−$BiVO_4$ (Figure 3a) showed the Ti 2p, Bi 4f, O 1s, and V 2p peaks, attributed to the typical elements of the composite. The peak at the binding energy of 980 eV was attributed to O KLL Auger peak at this energy.[20] The high-

DOI: 10.1021/acsami.7b07047
ACS Appl. Mater. Interfaces 2017, 9, 27185−27192

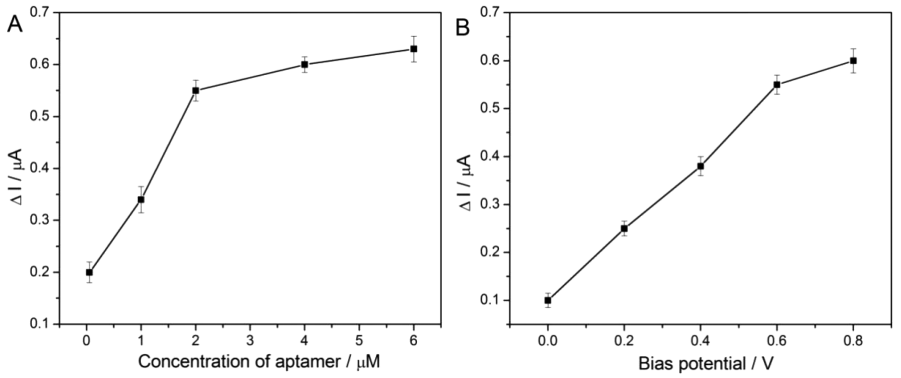

Figure 4. Influence of (A) aptamer concentration and (B) bias potential on PEC response of aptamer|TiO_2−$BiVO_4$|ITO to 60 pM E2 in 0.1 M PBS containing 0.1 M AA.

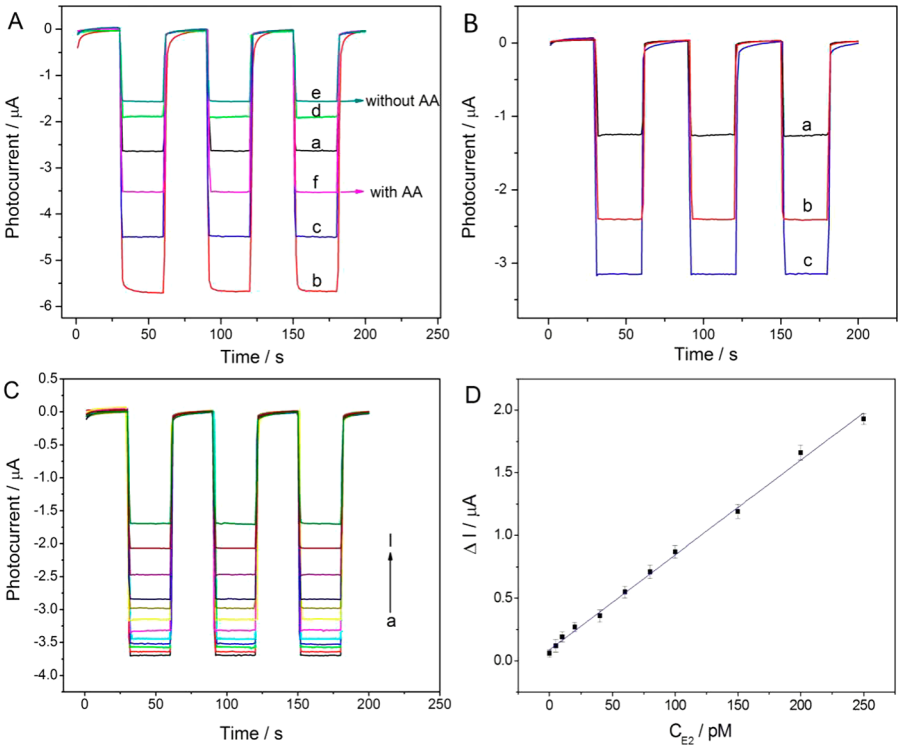

Figure 5. (A) Photocurrents at (a) TiO_2|ITO, (b) $BiVO_4$|ITO, (c) TiO_2−$BiVO_4$|ITO, (d) aptamer|TiO_2−$BiVO_4$|ITO in 0.1 M PBS (pH 7.4), and aptamer|TiO_2−$BiVO_4$|ITO in 0.1 PBS (pH 7.4) containing 10 pM E2 before (e) and after (f) addition of 0.1 M AA. (B) Photocurrents at (a) aptamer|TiO_2|ITO, (b) aptamer|$BiVO_4$|ITO, and (c) aptamer|TiO_2−$BiVO_4$|ITO in 0.1 M PBS (pH 7.4) containing 60 pM E2 and 0.1 M AA. (C) Photocurrent at PEC aptasensor in PBS (0.1 M, pH 7.4) containing 0, 0.1, S, 10, 20, 40, 60, 80, 100, 150, 200, and 250 pM E2 (from a to l) in the presence of 0.1 M AA at a bias voltage of +0.6 V. (D) Plot of Δ*I* and E2 concentration from 0.1 to 250 pM.

resolution spectrum of Ti 2p exhibited two peaks at 464.4 and 458.6 eV (Figure 3b), which could be assigned to Ti $2p_{1/2}$ and Ti $2p_{3/2}$ of Ti^{4+} in anatase titania.[11] In Figure 3c, two bands at 164.4 and 159.1 eV could be ascribed to the Bi $4f_{5/2}$ and Bi $4f_{7/2}$ binding energies, respectively, which confirmed that the bismuth species in the composite belonged to Bi^{3+} cations.[12] The asymmetric O 1s signal (Figure 3d) indicated the presence of different oxygen species on the surface of the sample, and the bands at 529.8 and 531.4 eV could be attributed to the surface lattice oxygen of TiO_2 and $BiVO_4$,[13] respectively. In Figure 3e, the vanadium peaks centered at the binding energies of 516.6 (V $2p_{3/2}$) and 523.9 (V $2p_{1/2}$) eV demonstrated the existence of the characteristic V^{5+} oxidation state in the composite.[21] In summary, the XPS spectra validated the formation of the $BiVO_4$ crystal on TiO_2.

Optimization of Aptasensor Preparation and Detection Potential. The response of the fabricated aptamer|TiO_2−$BiVO_4$|ITO sensor to E2 was optimized in 0.1 M PBS. Figure 4A illustrates that the PEC response of the aptasensor is obviously affected by the concentration of aptamer immobilized on the electrode. Specifically, the PEC response difference ($\Delta I = I - I_0$, I_0 is the blank photocurrent) toward E2 markedly increased with the increase of aptamer concentration up to 2 μM probably because the higher concentration of the aptamer immobilized on the electrode could capture more E2 molecules. However, the Δ*I* reached a platform when the aptamer concentration exceeded 2 μM, which could be ascribed to the steric hindrance of excessive aptamer retarding the electron transfer.[22] Consequently, the aptamer at 2 μM was chosen to fabricate the sensor. Meanwhile, the bias potential

DOI: 10.1021/acsami.7b07047
ACS Appl. Mater. Interfaces 2017, 9, 27185−27192

Table 1. Analytical Performance of Different Sensors for the Detection of E2

sensors	analytical technique	linear range/pM	LOD/pM	refs
TiP@Cd^{2+}/ITO[a]	PEC	$18-1.4 \times 10^4$	7.3	2
aptamer/AuNPs[b]/WS_2[c]/GCE[d]	DPV	$10-5.0 \times 10^3$	2.0	3
aptamer/CdSe-TiO_2	PEC	0.05−15	3.3×10^{-2}	4
aptamer/α-Fe_2O_3−NG[e]-AuNRs/ITO	PEC	$1.0 \times 10^{-3}-1.0 \times 10^3$	3.3×10^{-4}	5
Ag/PAMAM[f]-Au/GR[g]-PANI[h]/GCE	DPV	$1.4 \times 10^2-2.5 \times 10^4$	72	7
CdSe−BSA−E2/GCE	DPASV	$1.8 \times 10^2-3.67 \times 10^3$	1.8×10^2	8
cDNA/aptamer/AuNPs/CoS/GCE	DPV	1−1000	0.7	9
aptamer/AuNPs/PEDOT[i]/Au	SWV	$100-1 \times 10^5$	20	10
aptamer/Au	EIS	$10-1 \times 10^4$	2.0	11
aptamer|TiO_2−$BiVO_4$| ITO	PEC	0.1−250	2.5×10^{-2}	this work

[a]Cd^{2+}-functionalized titanium phosphate nanoparticles. [b]Au nanoparticles. [c]Layered tungsten disulfide. [d]Glassy carbon electrode. [e]N-doped graphene. [f]Poly(amino-amine) dendrimers. [g]Graphene. [h]Polyaniline;. [i]Poly(3,4-ethylenedioxylthiophene).

also showed an obvious effect on the PEC response of the sensor (Figure 4B). The response rapidly increased with enhancing the bias potential from +0.2 to +0.6 V because a larger anodic bias potential will push more photogenerated electrons to the counter electrode and reduce the recombination of hole−electron pairs more effectively, leading to higher photocurrent. However, the enhancement of the PEC response was significantly slowed down at an applied potential higher than +0.6 V, and therefore, +0.6 V was selected as the optimum applied potential for PEC sensing to minimize the interference arising from the high potentials.

Analytical Performance of PEC Aptasensor. The PEC performance of different modified ITO electrodes was evaluated by studying the photocurrents generated by irradiating the electrodes with intermittent visible incident light (Figure 5A). The photocurrent at TiO_2−$BiVO_4$|ITO (curve c) was ∼1.8 times larger than that at TiO_2|ITO (curve a), attributed to the fact that $BiVO_4$ particles has extended the absorption of TiO_2 spheres into the visible light region. In the composite, the conduction band edge potential of $BiVO_4$ (∼−0.7 eV) was more negative than that of TiO_2 (∼−0.4 eV),[23] so that the photoinduced electrons on the conduction band of $BiVO_4$ was easily transferred to that of TiO_2 to improve the PEC conversion efficiency of TiO_2.[24] However, the photocurrent at TiO_2−$BiVO_4$|ITO (curve c) is lower than that at $BiVO_4$|ITO (curve b), which can be explained by the substantial charge carrier loss of $BiVO_4$ on the TiO_2 nanospheres.[25] Noticeably, aptamer|TiO_2−$BiVO_4$|ITO (curve d) displays the lowest photocurrent among all of the modified electrodes owing to the steric hindrance of the biological molecules on ITO. The steric hindrance of the biomolecules retarded the movement of photogenerated electrons to ITO and thus increased their recombination with the holes. After 0.1 M AA was added in PBS (pH 7.4) containing 10 pM E2, the photocurrent at aptamer|TiO_2−$BiVO_4$|ITO was almost doubled (curve e and f), which was ascribed the fact that AA served as a scavenger of photogenerated holes to enhance and stabilize the photocurrent at the PEC aptasensor. To reduce the irradiation absorbance of AA at high concentration, 0.1 M AA was chosen for the subsequent test.

Compared to aptamer|TiO_2|ITO and aptamer|$BiVO_4$|ITO, aptamer|TiO_2−$BiVO_4$|ITO showed the highest photocurrent in PBS containing 60 PM of E2 (Figure 5B), indicating that the TiO_2−$BiVO_4$ heterostructure significantly enhanced the PEC efficiency for aptasensing. The result could be attributed to the strong visible-light excitation capability, high specific surface area, and excellent biocompatibility of the TiO_2−$BiVO_4$ heterostructure.

To evaluate the performance of the E2 PEC aptasensor, the photocurrent change was measured at various concentrations of E2. As shown in Figure 5C, the photocurrent gradually decreased with increasing concentrations of E2. Ascribed to the specific recognition reaction between E2 and aptamer, the E2−aptamer complexes were formed on the PEC sensing interface, which increased the steric hindrances for the diffusion of the electron donor and thus decreased the photocurrent. The plot of ΔI vs E2 concentration showed a linear relationship (Figure 5D). The photocurrent changed linearly with the concentration of E2 in the range from 0.1 to 250 pM (correlation coefficient of 0.998) with a detection limit of 0.022 pM (S/N = 3). The performance of the as prepared PEC sensor was superior to those of many other sensors (Table 1), which could be attributed to the excellent property of the TiO_2−$BiVO_4$ composite.

The PEC mechanism of the biosensing strategy is illustrated in Scheme 1B based on interparticle electron transfer behavior. The band edge positions of the conduction band (CB) and valence band (VB) of a semiconductor could be estimated according to the equation $E_{CB} = \chi - E^0 - 1/2E_g$, where χ is the absolute electronegativity of the compound, E^0 is the energy of free electron on the hydrogen scale, and E_g is the band gap of the semiconductor.[23] From Figure 2B, the band gaps of TiO_2 and $BiVO_4$ were calculated to be 3.2 and 2.34 eV, respectively. Therefore, the CB and VB edges of TiO_2 were calculated to be −0.2 and +3.0 eV, and those of $BiVO_4$ were 0.37 and 2.71 eV, respectively. After $BiVO_4$ and TiO_2 were joined to form a heterostructure, the Fermi levels of two components tended to a balanced value due to the charge redistribution and system thermal equilibrium.[26,27] Consequently, both the CB and VB of $BiVO_4$ moved to the positions negative to those of TiO_2,[28,29] facilitating the migration of the photogenerated electrons of $BiVO_4$ to the CB of TiO_2 and then to the ITO electrodes. Meanwhile, the photoinduced holes on the VB of TiO_2 could also be injected into that of $BiVO_4$ and then captured by an electron donor AA. The effective separation between the electrons and holes in the composite maintained the photocurrent stability of the PEC aptasensor, leading to a much better PEC performance of the TiO_2−$BiVO_4$ composite than that of pristine TiO_2 nanomaterials.

Stability, Specificity, and Practical Application. The stability of the PEC aptasensor was evaluated through monitoring the repeated photoexcited process 7 times over 420 s. In 0.1 mol L^{-1} PBS (pH 7.4), the photocurrent did not

DOI: 10.1021/acsami.7b07047
ACS Appl. Mater. Interfaces 2017, 9, 27185−27192

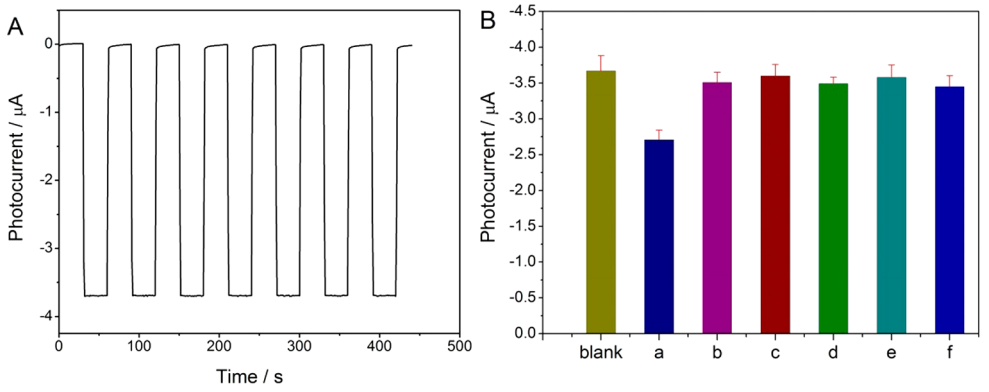

Figure 6. (A) Time based photocurrent response of aptamer|TiO_2−$BiVO_4$|ITO under several on/off irradiation cycles for 420 s. (B) The photocurrent of the prepared PEC E2 aptasensor to (a) 10 pM E2, and 50 pM of (b) estriol, (c) 1-aminoanthraquinone, (d) ethinylestradiol, (e) testosterone, and (f) bisphenol A.

show any obvious change at a bias voltage of 0.6 V under the irradiation, indicating the high stability of the PEC sensor (Figure 6A). The selectivity evaluation of the PEC aptasensor for 17β-estradiol was performed by testing the response of the sensor to some other common coexisted species including estriol, 1-aminoanthraquinone, ethinylestradiol, testosterone, and bisphenol A. The influences of these potential interferences on the determination of E2 were less than 6.7% (Figure 6B), indicating the high selectivity of the PEC aptasensor for E2.

The long-term storage stability of the aptamersensor was investigated after storing the aptamersensor in a refrigerator at 4 °C. The aptamersensor retained 92.5% and 86.5% of the initial response after 2 and 4 weeks of refrigerator storage, respectively. The good stability of the sensor was attributed to tight immobilzation of aptamer on the biocompatible sensor scaffold, which could retain the biological activity of biological molecules.

The practical application of the developed biosensor was studied by detecting 17β-estradiol in human urine samples collected from three volunteers. The human urine samples were diluted 100 times with PBS, and the standard addition method was used to quantitative analyze these samples. As listed in Table 2, the recoveries of the proposed method for these urine samples are in the range from 96.4 to 103.2%, demonstrating that the proposed sensor could be applied in practical determination of 17β-estradiol.

Table 2. Determination of 17β-Estradiol in Urine Samples (n = 3)

samples	spiked (pM)	found (pM)	RSD (%)	recovery (%)
1	5	4.82	1.6	96.4
	15	15.22	2.4	100.3
	30	30.17	1.9	99.4
2	5	5.27	3.2	101.2
	15	15.28	2.6	100.5
	30	30.31	2.8	100.3
3	5	5.07	3.5	98.4
	15	15.05	2.4	99.3
	30	30.96	3.0	103.2

CONCLUSION

We have prepared a TiO_2−$BiVO_4$ sphere heterostructure to develop a PEC aptamersensor, which displays high sensitivity, selectivity, and stability for simple and rapid determination of 17 β-estradiol. In the designed heterostructure, TiO_2 nanospheres provide a biocompatible microenvironment to maintain the aptamer bioactivity, and the high surface area of the heterostructure enhances the loading of aptamer molecules. The advantages of the nanocomposite with strong visible light absorption lead to high PEC efficiency for sensitive biosensing. The fabricated PEC aptasensor possesses excellent analytical performance and indicates that the TiO_2−$BiVO_4$ heterostructure is a promising candidate for the preparation of PEC biosensors.

AUTHOR INFORMATION

Corresponding Authors

*E-mail: xq_liu1975@yahoo.com.

*Phone/Fax: +86-25-89683593. E-mail: hxju@nju.edu.cn.

ORCID

Huangxian Ju: 0000-0002-6741-5302

Notes

The authors declare no competing financial interest.

ACKNOWLEDGMENTS

This work was financially supported by National Natural Science Foundation of China (Nos. U1504215 and 21576071), International Science and Technology Cooperative Project funded by The Department of Science and Technology of Henan Province (172102410042), and the Scientific Research Foundation for the Returned Overseas Chinese Scholars, State Education Ministry Batch 46th.

REFERENCES

(1) Fan, L.; Zhao, G.; Shi, H.; Liu, M.; Wang, Y.; Ke, H. A Femtomolar Level and Highly Selective 17β-Estradiol Photoelectrochemical Aptasensor Applied in Environmental Water Samples Analysis. *Environ. Sci. Technol.* **2014**, *48*, 5754−5761.

(2) Li, R.; Liu, Y.; Yan, T.; Li, Y.; Cao, W.; Wei, Q.; Du, B. A Competitive Photoelectrochemical Assay for Estradiol Based on in Situ Generated Cds-Enhanced TiO_2. *Biosens. Bioelectron.* **2015**, *66*, 596−602.

(3) Chang, H.-S.; Choo, K.-H.; Lee, B.; Choi, S.-J. The Methods of Identification, Analysis, and Removal of Endocrine Disrupting Compounds (EDCs) in Water. *J. Hazard. Mater.* **2009**, *172*, 1−12.

(4) Wang, G.-L.; Jiao, H.-J.; Liu, K.-L.; Wu, X.-M.; Dong, Y.-M.; Li, Z.-J.; Zhang, C. A Novel Strategy for the Construction of Photoelectrochemical Sensors Based on Quantum Dots and Electron

DOI: 10.1021/acsami.7b07047
ACS Appl. Mater. Interfaces 2017, 9, 27185−27192

Acceptor: The Case of Dopamine Detection. *Electrochem. Commun.* **2014**, *41*, 47−50.
(5) Hu, Y.; Xue, Z.; He, H.; Ai, R.; Liu, X.; Lu, X. Photoelectrochemical Sensing for Hydroquinone Based on Porphyrin-Functionalized Au Nanoparticles on Graphene. *Biosens. Bioelectron.* **2013**, *47*, 45−49.
(6) Giordano, F.; Abate, A.; Correa Baena, J. P.; Saliba, M.; Matsui, T.; Im, S. H.; Zakeeruddin, S. M.; Nazeeruddin, M. K.; Hagfeldt, A.; Graetzel, M. Enhanced Electronic Properties in Mesoporous TiO_2 Via Lithium Doping for High-Efficiency Perovskite Solar Cells. *Nat. Commun.* **2016**, *7*, 10379.
(7) Yildirim, N.; Long, F.; Gao, C.; He, M.; Shi, H.-C.; Gu, A. Z. Aptamer-Based Optical Biosensor for Rapid and Sensitive Detection of 17β-Estradiol in Water Samples. *Environ. Sci. Technol.* **2012**, *46*, 3288−3294.
(8) Li, H.; Wang, D.; Fan, H.; Jiang, T.; Li, X.; Xie, T. Synthesis of Ordered Multivalent Mn-TiO_2 Nanospheres with Tunable Size: A High Performance Visible-Light Photocatalyst. *Nano Res.* **2011**, *4*, 460−469.
(9) Abdi, F. F.; Han, L.; Smets, A. H. M.; Zeman, M.; Dam, B.; van de Krol, R. Efficient Solar Water Splitting by Enhanced Charge Separation in a Bismuth Vanadate-Silicon Tandem Photoelectrode. *Nat. Commun.* **2013**, *4*, 2195.
(10) Ding, C.; Qin, W.; Wang, N.; Liu, G.; Wang, Z.; Yan, P.; Shi, J.; Li, C. Solar-to-Hydrogen Efficiency Exceeding 2.5% Achieved for Overall Water Splitting with an All Earth-Abundant Dual-Photoelectrode. *Phys. Chem. Chem. Phys.* **2014**, *16*, 15608−15614.
(11) Sun, S.; Wang, W.; Zhou, L.; Xu, H. Efficient Methylene Blue Removal over Hydrothermally Synthesized Starlike $BiVO_4$. *Ind. Eng. Chem. Res.* **2009**, *48*, 1735−1739.
(12) Yehezkeli, O.; Harguindey, A.; Domaille, D. W.; He, L.; Cha, J. N. Synthesis and Phase Transfer of Well-Defined $BiVO_4$ Nanocrystals for Photocatalytic Water Splitting. *RSC Adv.* **2015**, *5*, 58755−58759.
(13) Shu, J.; Qiu, Z.; Lin, Z.; Cai, G.; Yang, H.; Tang, D. Semiautomated Support Photoelectrochemical Immunosensing Platform for Portable and High-Throughput Immunoassay Based on Au Nanocrystal Decorated Specific Crystal Facets $BiVO_4$ Photoanode. *Anal. Chem.* **2016**, *88*, 12539−12546.
(14) Huang, K.-J.; Liu, Y.-J.; Zhang, J.-Z.; Cao, J.-T.; Liu, Y.-M. Aptamer/Au Nanoparticles/Cobalt Sulfide Nanosheets Biosensor for 17β-Estradiol Detection Using a Guanine-Rich Complementary DNA Sequence for Signal Amplification. *Biosens. Bioelectron.* **2015**, *67*, 184−191.
(15) Li, H.; Qiao, Y.; Li, J.; Fang, H.; Fan, D.; Wang, W. A Sensitive and Label-Free Photoelectrochemical Aptasensor Using Co-Doped ZnO Diluted Magnetic Semiconductor Nanoparticles. *Biosens. Bioelectron.* **2016**, *77*, 378−384.
(16) Ahour, F.; Ahsani, M. K. An Electrochemical Label-Free and Sensitive Thrombin Aptasensor Based on Graphene Oxide Modified Pencil Graphite Electrode. *Biosens. Bioelectron.* **2016**, *86*, 764−769.
(17) Tsai, M.-C.; Tsai, T.-L.; Shieh, D.-B.; Chiu, H.-T.; Lee, C.-Y. Detecting HER2 on Cancer Cells by TiO_2 Spheres Mie Scattering. *Anal. Chem.* **2009**, *81*, 7590−7596.
(18) Jung, H.; Chae, S. Y.; Shin, C.; Min, B. K.; Joo, O.-S.; Hwang, Y. J. Effect of the Si/TiO_2/$BiVO_4$ Heterojunction on the Onset Potential of Photocurrents for Solar Water Oxidation. *ACS Appl. Mater. Interfaces* **2015**, *7*, 5788−5796.
(19) Li, X.; Zhang, Z.; Zhang, F.-J.; Liu, J.; Ye, J.; Oh, W.-C. Synthesis and Photocatalytic Activity of TiO_2/$BiVO_4$ Layered Films under Visible Light Irradiation. *Han'guk Seramik Hakhoechi* **2016**, *53*, 665−669.
(20) Zong, M.; Huang, Y.; Wu, H.; Zhao, Y.; Wang, Q.; Sun, X. One-Pot Hydrothermal Synthesis of RGO/$CoFe_2O_4$ Composite and Its Excellent Microwave Absorption Properties. *Mater. Lett.* **2014**, *114*, 52−55.
(21) Chen, D.; Huang, F.; Cheng, Y.-B.; Caruso, R. A. Mesoporous Anatase TiO_2 Beads with High Surface Areas and Controllable Pore Sizes: A Superior Candidate for High-Performance Dye-Sensitized Solar Cells. *Adv. Mater. (Weinheim, Ger.)* **2009**, *21*, 2206−2210.
(22) Liu, Y.; Yan, K.; Okoth, O. K.; Zhang, J. A Label-Free Photoelectrochemical Aptasensor Based on Nitrogen-Doped Graphene Quantum Dots for Chloramphenicol Determination. *Biosens. Bioelectron.* **2015**, *74*, 1016−1021.
(23) Sun, J.; Li, X.; Zhao, Q.; Tade, M. O.; Liu, S. Quantum-Sized $BiVO_4$ Modified TiO_2 Microflower Composite Heterostructures: Efficient Production of Hydroxyl Radicals Towards Visible Light-Driven Degradation of Gaseous Toluene. *J. Mater. Chem. A* **2015**, *3*, 21655−21663.
(24) Zhang, L.; Tan, G.; Wei, S.; Ren, H.; Xia, A.; Luo, Y. Microwave Hydrothermal Synthesis and Photocatalytic Properties of TiO_2/$BiVO_4$ Composite Photocatalysts. *Ceram. Int.* **2013**, *39*, 8597−8604.
(25) Wang, R.; Bai, J.; Li, Y.; Zeng, Q.; Li, J.; Zhou, B. $BiVO_4$/$TiO_2(N_2)$ Nanotubes Heterojunction Photoanode for Highly Efficient Photoelectrocatalytic Applications. *Nano-Micro Lett.* **2017**, *9*, 14−19.
(26) Hu, Y.; Li, D.; Zheng, Y.; Chen, W.; He, Y.; Shao, Y.; Fu, X.; Xiao, G. $BiVO_4$/TiO_2 Nanocrystalline Heterostructure: A Wide Spectrum Responsive Photocatalyst Towards the Highly Efficient Decomposition of Gaseous Benzene. *Appl. Catal., B* **2011**, *104*, 30−36.
(27) Sun, J.; Li, X.; Zhao, Q.; Ke, J.; Zhang, D. Novel V_2O_5/$BiVO_4$/TiO_2 Nanocomposites with High Visible-Light-Induced Photocatalytic Activity for the Degradation of Toluene. *J. Phys. Chem. C* **2014**, *118*, 10113−10121.
(28) Zhang, C.; Guo, D.; Xu, W.; Hu, C.; Chen, Y. Radiative/Nonradiative Recombination Affected by Defects and Electron−Phone Coupling in $CdWO_4$ Nanorods. *J. Phys. Chem. C* **2016**, *120*, 12218−12225.
(29) Zhang, C.; Zhang, H.; Zhang, K.; Li, X.; Leng, Q.; Hu, C. Photocatalytic Activity of Znwo4: Band Structure, Morphology and Surface Modification. *ACS Appl. Mater. Interfaces* **2014**, *6*, 14423−14432.

DOI: 10.1021/acsami.7b07047
ACS Appl. Mater. Interfaces 2017, 9, 27185−27192